Numerical study of P3HT-based hybrid solid-state quantum dot solar cells with CdS quantum dots employing different metal oxides using SCAPS-1D

M. Seddar Yagoub* and M. Adnane

Laboratoire de Microscopie Electronique et Sciences des Matériaux,
Département de Technologie des Matériaux, Faculté de physique,
Université des Sciences et de la Technologie d'Oran Mohamed Boudiaf USTO,
USTO-MB, Oran, 31000, Algeria.
* *mohamedseddar111@gmail.com*
ORCID number: 0000-0002-3252-4744

Received 12 December 2023; accepted 20 June 2024

This study presents a comprehensive numerical investigation into solid-state quantum dot solar cells (SSQDSCs) utilizing P3HT poly(3-hexylthiophene) as both a hole transport and absorber layer employing SCAPS-1D simulation software, the research explores the performance of cells composed of FTO (Fluorine-doped Tin Oxide) as the front contact, integrated with different metal oxides (Titanium dioxide (TiO_2), zinc oxide (ZnO), and tin dioxide (SnO_2), CdS (Cadmium sulfide) quantum dots, P3HT, and Pt (platinum) as the back contact namely Hybrid solar cell. The thickness of each layer is systematically optimized, and the influence of various CdS quantum dots sizes is thoroughly examined. The study also dived into the characterization of interface defects at the P3HT/CdS junction, involving modifications to the electron affinity of P3HT. Additionally, the impact of metal work function variations was also investigated analyzing at each case critical parameters such as open-circuit voltage (V_{OC}), short-circuit current density (J_{SC}), fill factor (FF), power conversion efficiency (PCE), and quantum efficiency. The results demonstrate that optimization of these parameters has the potential to elevate solar cell efficiency to 18%. These simulation findings offer valuable insights for comparative analysis and a deeper understanding of the challenges encountered in experimental research.

Keywords: CdS quantum dots; P3HT; Hybrid Solar cell; SCAPS 1D.

DOI: https://doi.org/10.31349/RevMexFis.70.061001

1. Introduction

The exponential growth of the world's population has resulted in an increase in energy demand to support normal activities [1], pushing the scientific community to step up its efforts. The growing need to handle expanding energy demands has pushed academics to pursue alternative sources of energy. Solar energy has emerged as an exceptionally promising route among these exploratory efforts due to its inherent renewability and widespread availability [2]. The progression of solar energy research has resulted in the concept of three different "generations," each representing a different stage of technological achievement [3]. Notably, the third generation involves an array of cutting-edge possibilities, which includes quantum dots solar cells. These nanostructured devices have attracted scientific researchers, opening up opportunities for the advancement of solar technology [4]. Over the last decades, significant research efforts have been dedicated to quantum dot-sensitized solar cells (QDSCs) [5]. These photovoltaic devices hold substantial promise as one of the most prospective solar cell types, capitalizing on the unique benefits afforded by semiconductor quantum dots (QDs). Notably, these sensitizing nanocrystals (NCs) offer a range of crucial attributes, including size-tunable bandgap energy [6], the potential for multiple exciton generation [7], a high absorption coefficient [8], and the capability to absorb a wide spectrum of wavelengths [9]. Of particular significance, these attributes contribute to the distinctiveness of QDSCs. Moreover, the quantum confinement effects play a transformative role by altering the physical properties of the sensitizing film, imparting quantum dots-sensitized solar cells with enhanced functionalities and efficiencies [10]. Among the quantum dots semiconductor materials, Cadmium sulphide (CdS) holds particular significance. It is classified as a compound semiconductor with n-type conductivity and stands out for its noteworthy characteristics, including high transparency [11], a direct bandgap transition of 2.4 eV [12], and a notably efficient electron affinity of 4.2 eV [13]. The utilization of CdS offers the additional advantage of improving the interface match at the lattice heterojunction, enhancing the lifetime of additional carriers, and optimizing the band alignment within the device structure [14]. The deposition of CdS quantum dots can be achieved through various techniques, such as direct attachment [15], electrodeposition [16], and successive ionic layer adsorption and reaction (SILAR) [17]. Despite their promising potential to enhance light absorption and overall efficiency, quantum dot solar cells (QDSCs) incorporating liquid electrolytes have encountered a significant challenge. The use of liquid electrolytes introduces issues related to leakage, evaporation, and long-term stability, limiting the practicality and durability of these devices [18]. However, a promising solution lies in the adoption of solid-state electrolytes and p-type inorganic or organic semiconductors that can overcome the drawbacks

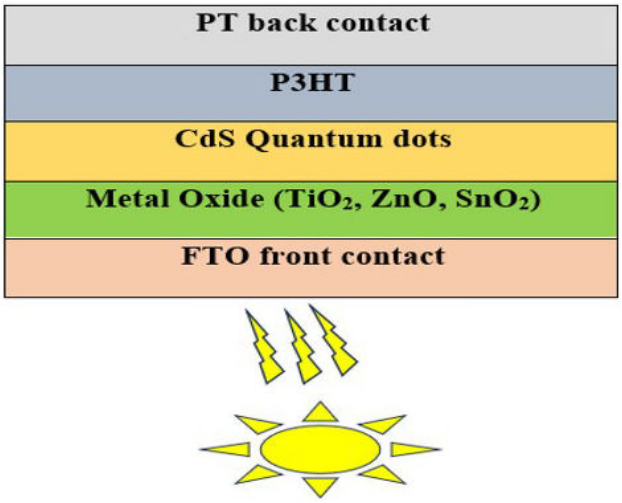

FIGURE 1. The structure of the proposed Hybrid solar cell.

associated with liquid counterparts by providing enhanced stability [19], reduced leakage risks, and improved resistance to environmental factors. By transitioning from liquid to solid-state quantum dot solar cells (SSQDSCs) can obtain more reliable and long-lasting performance, paving the way for their practical integration into renewable energy systems [20]. Organic semiconductors functioning as hole transport materials (HTMs) have garnered significant research attention, with notable examples including Spiro-OMeTAD, PTAA (poly-triaryl amine), PEDOT: PSS(poly(3,4-ethylenedioxythiophene) polystyrene sulfonate) and P3HT. Similarly, inorganic semiconductors like CuSCN (copper(i) thiocyanate) and CuOx (copper oxides) have also been extensively investigated in this regard [21,22]. P3HT, as a p-type semiconductor, has captured the interest of numerous researchers due to its remarkable light-absorbing and hole-transporting characteristics. This has paved the way for the development of a novel type of solar cell known as Hybrid Solar cells [23,24].

This paper employs SCAPS simulation to investigate the efficiency of a solar cell with the following architecture: FTO utilized as the front contact, incorporating well-researched metal oxides such as TiO_2, ZnO, and SnO_2 as electron transport materials (ETMs), along with CdS quantum dots and P3HT. The back contact is composed of Pt as illustrated in Fig. 1. The selection of this particular structure is guided by extensive prior experimental research into this specific configuration, as documented in Refs. [25-27]. This simulation study aids in comprehending the challenges and limitations associated with low efficiency [28,29]. It demonstrates that by integrating quantum dots with optimized parameters, it is possible to achieve an efficiency level of 18%. To the best of our current knowledge, this study appears to be the first to combine these materials within a SCAPS-1D simulation for the analysis of hybrid solar cells featuring this specific structure, employing different quantum dot band gaps. It also demonstrates the enhancement of ohmic contact by altering the electron affinity of P3HT. Additionally, the study reveals that interface defects play a crucial role in preventing the occurrence of S-shaped J-V curves. By addressing these aspects, the research provides new insights into optimizing the performance and stability of hybrid solid-state solar cells, significantly advancing photovoltaic technology.

2. Computational methodology and device structure

The study relies on the utilization of Solar Cell Capacitance Simulator (SCAPS-1D) version 3.3.10 for conducting all numerical computations presented herein. Numerical simulation plays a foundational role in the formulation, exploration, and projection of the actual photovoltaic (PV) device characteristics. This approach also furnishes valuable insights into the manipulation and enhancement of solar cell performance through adjustments in geometric and technical attributes. The software package possesses the capability to model up to seven layers and offers the flexibility to fine-tune various input parameters-such as doping concentration, relative permittivity, electron affinity, thickness, mobility, and defect concentrations-to optimize the efficiency of the solar cell. Additionally, the software proficiently resolves fundamental semiconductor equations, as well as Poisson's and continuity equations, under conditions of steady-state operation. Simulation reports play a vital role in minimizing the costs associated with fabrications. They offer deeper insights into internal processes and enable the determination of parameters that might be challenging to ascertain through experimentation. Thanks to its user-friendly interface and a wide range of simulation techniques, SCAPS emerges as the favored option for such tasks. The optimization of the hybrid solar cell structure was achieved through comprehensive simulations. In this process, the thicknesses of both the Electron Transport Layers (ETLs) using most studies metal oxides (TiO_2, ZnO, SnO_2) [30-32] and the Hole Transport and absorber layer P3HT Layer were systematically varied to attain the highest efficiencies. Moreover, the band gap of CdS quantum dots was varied due to quantum confinement effects. This modification influenced parameters such as density of states [33] and electron affinity [34,35], leading to intricate alterations. The electron affinity of P3HT was also subject to variation. Additionally, the interface defect density between CdS quantum dots and P3HT was manipulated. Furthermore, the work function of the back contact was explored as a parameter influencing device performance. Notably, the initial testing phase encompassed the exploration of other p-type semiconductors like spiro-OMeTAD, CuSCN, and NiO (nickel oxide). However, spiro-OMeTAD exhibited a notably low Power Conversion Efficiency (PCE) of around 1.1%, while CuSCN and NiO exhibited non-convergence due to band alignment mismatches. It is crucial to highlight that interface defects play a pivotal role in avoiding the occurrence of S-shaped J-V curves, a phenomenon that has been experimentally observed [36]. Moreover, the incorporation

TABLE I. List of physical and electronic properties for each layer parameter.

Parameters	TiO_2 [39,40]	SnO_2 [41,42]	ZnO [43,44]	CdS [11,15,43,45]	P3HT [40,46]
Thickness (nm)	500 (Varied)	500 (Varied)	500 (Varied)	40 (Varied)	1000 (Varied)
Electron affinity (eV)	4	4.3	4.3	4.2 (Varied)	3.2 (Varied)
Dielectric permitivity (ε_r)	9	9	9	10	3
Effective conduction band density $N_c\ (cm^{-3})$	2.2E + 18	2.2E + 18	2.2E + 18	2.2E + 18 (Varied)	2.2E + 18
Effective valence band density $N_v\ (cm^{-3})$	1.8E + 19	2.2E + 18	2.2E + 18	2.2E + 18 (Varied)	2.2E + 18
Electron thermal velocity (cms^{-1})	1.00E + 07	1.00E + 07	1.00E + 07	1.00E + 07	1.00E + 07
Hole thermal velocity (cms^{-1})	1.00E + 07	1.00E + 07	1.00E + 07	1.00E + 07	1.00E + 07
Electron mobility $(cm^2\ V^{-1}\ s^{-1})$	20	260	166	360	10
Hole mobility $(cm^2\ V^{-1}\ s^{-1})$	10	10	20	40	2.8
Gap energy E_g (eV)	3.2	3.6	3.4	2.4 (Varied)	2.0
Donor concentration $N_d\ (cm^{-3})$	1.00E + 18	1.00E + 18	1.00E + 18	1.00E + 18	0
Acceptor concentration $N_a\ (cm^{-3})$	0	0	0	0	1.00E + 18
Total defect density (cm^{-3}) neutral	1.00E + 15	1.00E + 15	1.00E + 15	1.00E + 15	1.00E + 16

of a CdS layer was deemed essential in achieving convergence since with the P3HT/metal oxide combination and without this CdS layer, the band alignment mismatch hinders convergence with P3HT/metal oxide structures, potentially explaining the limited convergence observed in some reports [37,38]. In this study, priority was given to examining the impact of intrinsic material parameters on solar cell performance, leading to the intentional omission of shunt resistance variation. To maintain clarity and handle complexity, we assumed a constant high value for shunt resistance, while also treating defects and interface defects as analogous to shunt resistance. This methodology ensured a comprehensive analysis of the effects of intrinsic factors on performance. However, we acknowledge the importance of explicitly considering shunt resistance variation and propose it as a focal point for future research to enhance our understanding of solar cell behavior. The cell modeling utilized the AM1.5G spectrum at 300 K, with an incident solar power of 1000 W/m^2. Additionally, Table I provides a comprehensive overview of all operational parameters and numerical coefficients. For all simulations conducted in this software, the voltage scan range was set from 0 V to 2 V.

3. Results and discussion

3.1. Metal oxides thickness optimization

The study involved altering the thickness of metal oxide layers, specifically TiO_2, ZnO, and SnO_2, which play a crucial role in the performance of solar cells. The thickness variations ranged from 500 nm to 2000 nm. It is important to note that the P3HT layer and Bulk CdS layer remained unchanged according to the provided table. Additionally, the front and back contacts remained constant throughout the study. Notably, significant changes were observed in various solar cell measurements, including V_{OC}, FF, J_{sc}, and PCE. Remarkably, V_{OC} and FF displayed consistency across the range of thickness variations for all metal oxides. For TiO_2, V_{OC} was measured at 0.91 V, while for SnO_2 and ZnO, it was 0.92 V each. The FF hovered around 83% to 84% for all metal oxides (Fig. 2), aligning with previously reported results [47,48]. This suggests that changes in the thickness of the electron transport layer (ETL) have limited impact on these two properties. It implies that the ETL's thickness has minimal effect on charge carrier recombination and other losses within the cell because V_{OC} is primarily affected by the absorber layer (P3HT) and the energy level alignment between the absorber layer and the CdS layer [49]. Conversely, the fill factor FF is influenced by various factors related to the front and back contacts, as well as resistive losses within the solar cell. FF reflects the efficiency of retrieving generated current from the cell and is affected by series resistance, shunt resistance

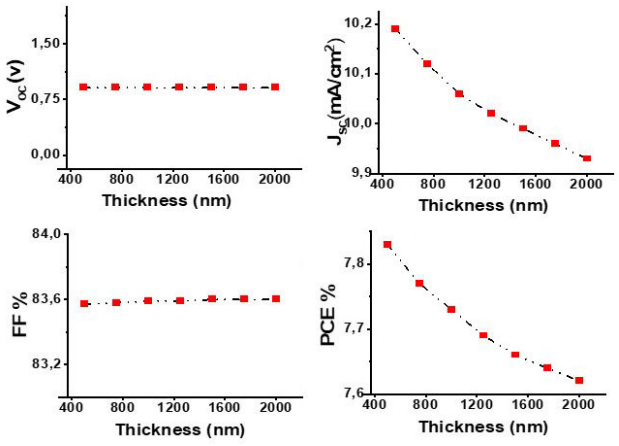

FIGURE 2. TiO_2 thickness variation with respect to V_{oc}, J_{sc}, FF and PCE.

(which was omitted for simplicity), and charge carrier recombination within the device [50,51]. Since our study kept the contacts (Pt and FTO) constant and observed no significant changes in other parameters that could impact FF, it remained stable across different metal oxide thicknesses. However, it was noted that both J_{sc} and PCE decreased with increasing ETL thickness. For instance, J_{sc} decreased from 10.19 mA/cm^2 to 9.93 mA/cm^2 for the TiO_2 layer, from 10.99 mA/cm^2 to 9.95 mA/cm^2 for the SnO_2 layer, and from 11 mA/cm^2 to 10.9 mA/cm^2 for the ZnO layer. In the case of PCE, it decreased from 7.83% to 7.62% for TiO_2, from 8.46% to 8.40% for ZnO, and from 8.41% to 8.36% for SnO_2. This behavior can be attributed to the increased absorption of light within the ETL layer itself, leading to a reduced availability of photons for absorption in the main absorber layer P3HT. Consequently, the generation of electron-hole pairs decreased, and the short-circuit current decreased as well. Moreover, increasing the thickness of the ETL extended the path of carriers from the photoactive layer to the electrode, thereby increasing carrier recombination and ohmic losses. These factors collectively contributed to the decrease in overall charge transport efficiency, which in turn affected the short-circuit current [52,53].

In addition to affecting J_{sc} and PCE, changes in the thickness of the metal oxide layers also had an impact on external quantum efficiency (QE). The QE spectra can be divided into two regions: below 400 nm and above 400 nm (Fig. 3). Above 400 nm, the response remained nearly identical for both thicknesses (500 nm and 1000 nm), mainly due to the consistent parameters of other layers. However, the response of solar cells decreased in the 300-375 nm range as the thickness of TiO_2, SnO_2, and ZnO increased. This is because as the thickness increased, less photons could be absorbed by the absorber layer, resulting in reduced samples responsiveness [54]. Furthermore, the higher bandgap of these thicker layers decreased the responsiveness at shorter wavelengths [55].

3.2. P3HT thickness optimization

Given that the P3HT layer functions as both the Hole Transport Layer (HTL) and Absorber layer, it becomes a pivotal factor in optimizing photovoltaic cells. Evaluating solar cell efficiency requires careful consideration of the thickness of this absorber layer. To enhance current density, the thickness must be meticulously adjusted [56,57]. Thinner absorber layers in solar cells result in reduced current densities and efficiency due to inadequate light absorption. Conversely, a thicker absorber layer creates a longer path for photogenerated charge carriers, which increases recombination but does not significantly benefit solar cell performance [58,59]. The thickness of the P3HT layer was varied from 500 nm to 2000 nm, while the metal oxide and bulk CdS layers remained unaltered. It is noteworthy that V_{OC} (open-circuit voltage) remains constant at 0.92 V throughout this range of thickness variations, and the fill factor (FF) experiences a slight decrease from 83.57% to 82.72%. However, the short circuit current (J_{sc}) and power conversion efficiency (PCE) increase up to a maximum value of 10.82 mA/cm^2 and 8.30%, respectively, between 500 nm and 1000 nm. Then, they gradually decrease from 1000 nm to 2000 nm (Fig. 4). This implies that V_{OC} stability is independent of the P3HT layer thickness and is more likely influenced by the P3HT layer's band alignment with the CdS layer. A stable V_{OC} can be achieved even with varying P3HT thicknesses if the band alignment allows effective charge carrier separation and minimizes recombination [60].

Additionally, it is important to consider that interface defects, which remain constant, also impact V_{OC} stability. According to Eq. (1) [61], a stable V_{OC} implies that the short circuit current (J_{sc}) is greater than the dark current (J_0) across the entire thickness range. This indicates that J_{sc} and J_0 vary linearly, a positive sign of effective light-induced current generation with minimal recombination or leakage. This underscores efficient charge separation and the system's ability to convert light energy into electrical current [62]. Regarding

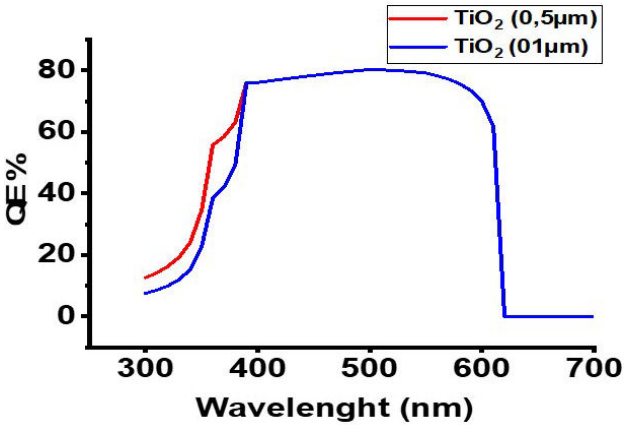

FIGURE 3. Quantum efficiency with respect to TiO_2 thickness variation.

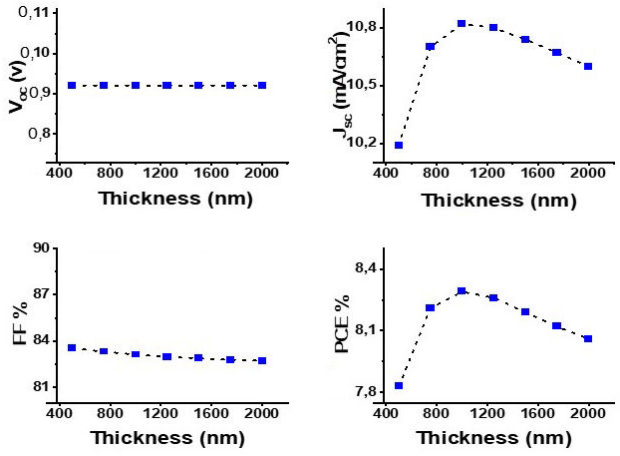

FIGURE 4. P3HT thickness variation with respect to V_{oc}, J_{sc}, FF and PCE.

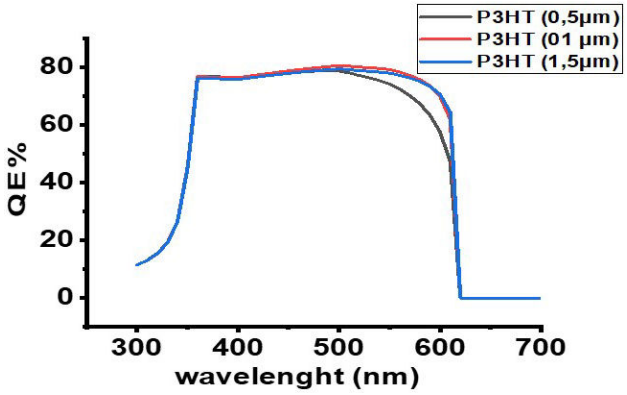

FIGURE 5. Quantum efficiency with respect to P3HT thickness variation.

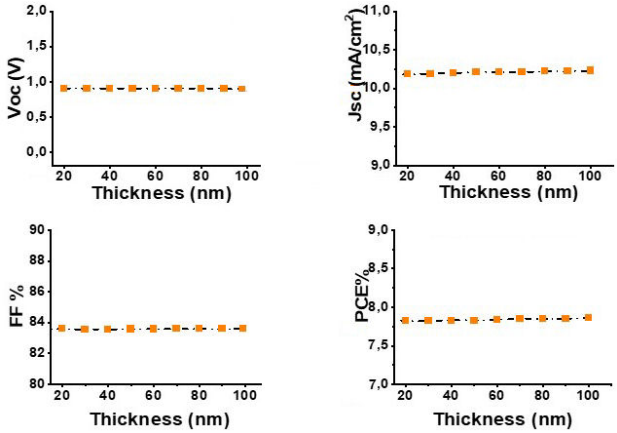

FIGURE 6. CdS thickness variation with respect to V_{OC}, J_{sc}, FF and PCE.

the quasi-stability of FF, it results from the device operating optimally, extracting the maximum available power while maintaining maximum voltage and current conditions. According to Eq. (2), maintaining FF constant implies that V_{OC} is approximately equal to V_{MPP} (maximum power voltage) and J_{sc} is approximately equal to J_{MPP} (current at maximum power point). This indicates that the device is operating efficiently and utilizing available energy effectively without compromising voltage potential. This alignment ensures that the device extracts its maximum attainable power without sacrificing current potential [63].

$$Voc = \frac{KBT}{q} \ln\left(\frac{J_{sc}}{J_0} + 1\right), \tag{1}$$

$$FF = \frac{V_{MPP}.J_{MPP}}{V_{oc}.J_{sc}}. \tag{2}$$

The thickness of the P3HT layer in solar cells significantly influences variations in J_{sc} and efficiency with thickness variation. This is attributed to changes in light absorption and charge carrier generation. An optimal thickness of 1000 nm strikes a balance between efficient charge transport to the electrodes and avoiding excessive carrier recombination [64]. Thicker P3HT layers may act as recombination centers, leading to reduced J_{sc} and efficiency due to a high defect density ($N_t = 10^{16}$ 1/cm^3) [65]. Additionally, excessive thickness may increase the distance that charge carriers need to travel to reach the electrodes, potentially resulting in higher recombination losses. The absorption profile of P3HT may also vary with thickness, affecting the path length of light within the device [66]. Apart from the changes in J_{sc} and PCE, there is a slight increase in quantum efficiency between 500 nm and 600 nm as the thickness of P3HT increases (Fig. 5). This indicates that a thicker layer enhances the conversion of photons into charge carriers within this wavelength range. The improved quantum efficiency can be attributed to better photon absorption and lower recombination losses [67].

3.3. CdS thickness optimization

To optimize the CdS layer thickness which was varied from 10 nm to 100 nm (Fig. 6), it could be noticed that there were no changes in V_{OC}, J_{sc}, FF, PCE and neither the quantum efficiency. The stability trend of these factors alongside thickness variation is the result of stable electron- hole pair generation. With increased buffer layer thickness, the same quantity of electron-hole pair can reach the active layer. Furthermore, due to its band gap of 2.4 ev, a 100 nm thick CdS layer does not absorb photons that could be passed into the active layer easily, hence holding efficiency constant [68-70].

3.4. The effect of CdS quantum dots layer on the performance of the solar cell

Due to the quantum confinement effect the band gap of CdS increases and other electronic parameters alter when the size of the quantum dot decreases where this change has consequences for the design and engineering of nanoscale materials for different application in electronics, optoelectronics, and photonics [71,72]. In our study, the band gap has been altered from the bulk CdS layer at 2.4 eV to quantum dot layers with band gaps of 2.6 eV, 2.8 eV, and 3.0 eV. These variations correspond to quantum dot sizes of approximately 3.1 nm, 2.3 nm, and 2.1 nm, respectively, as indicated in Ref. [73]. As it could be noticed that the V_{OC}, FF and PCE increase when CdS band gap increases for all metal oxides while the J_{sc} maintains stable, a larger band gap allows higher energy photons to be absorbed, resulting in a greater V_{OC} and overall efficiency as well as a fill factor [74]. This shows that increasing the band gap can potentially align the energy levels in semiconductor materials, reducing energy barriers that might hinder charge carrier transportation or increase recombination [75].

On the other hand, the stability of J_{sc} means the decreasing of dark current J_0 that suggests that the device has improved charge carrier mobility, collection efficiency, and reduced losses owing to non-radiative recombination since the

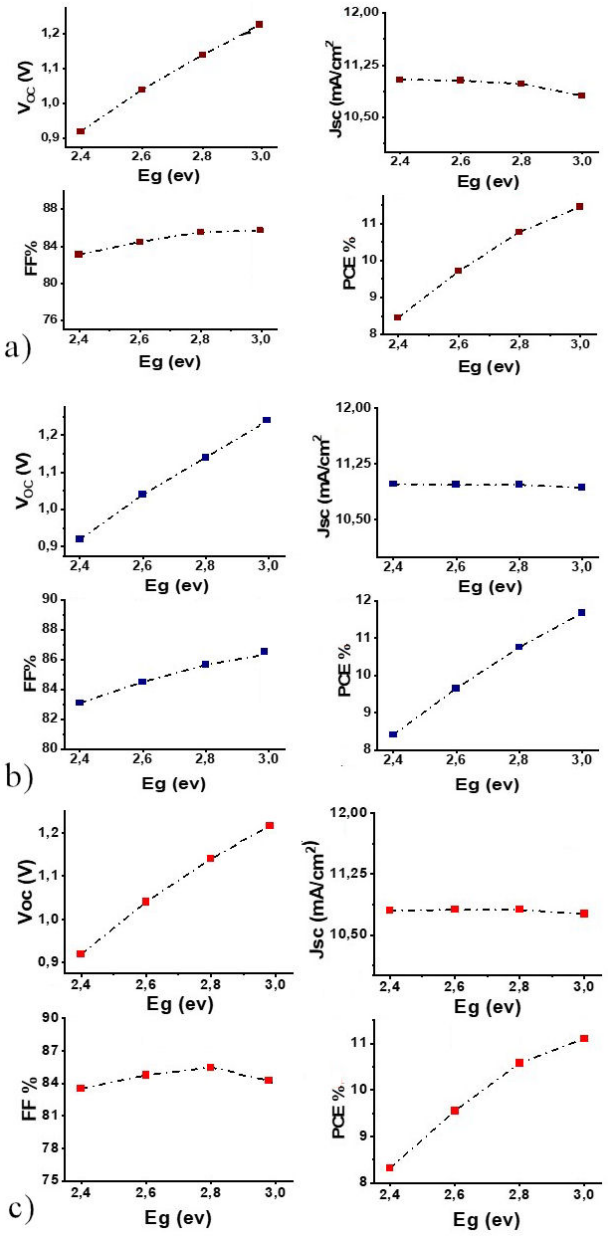

FIGURE 7. CdS Qds Eg variation with respect to V_{OC}, J_{sc}, FF and PCE for a) ZnO, b) SnO_2 and c) TiO_2.

quantum confinement affects the dark current [76,77]. The variation of V_{OC}, FF, J_{sc} and PCE as well as Quantum efficiency and I-V curve for TiO_2, ZnO, SnO_2 based solar cells are shown in Figs. 7, 8 and 9 for CdS bulk band gap and different CdS quantum dot band gaps. It can be observed that SnO_2 and ZnO show better performance than TiO_2 which is due to their higher electron mobility similar to [78]. However we can see that there is a slight decrease in quantum efficiency in the shorter wavelength 300 to 350 nm for all samples when moving from bulk CdS layer to CdS quantum dot layer which is due to the higher bandgap of these layers lowers responsiveness at short wavelengths suggesting that it contributes less to electron generation [79].

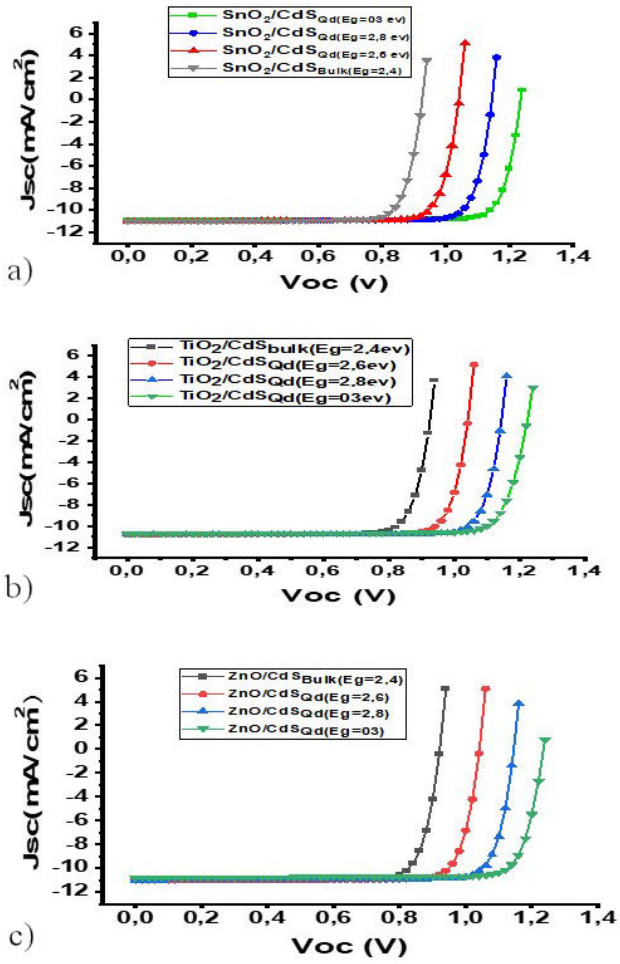

FIGURE 8. CdS Qds Eg variation with respect to I-V curve for ZnO, SnO_2 and TiO_2 based solar cells.

3.5. The effect of interface defect density

The appearance of various defects at the interface causes multiple traps and recombination centers within the bandgap, along with undesirable band bending [80]. In this study, the interface defect density of P3HT/CdS is varied. This variation has shown a remarkable change in solar cell efficiency and other parameters, unlike the interface defects of CdS/metal oxides, which resulted in a slight change of only 0.08% in PCE. The simulation was conducted to vary the interface defect density within the range of 10^{11} (1/cm^2) to 10^{16} (1/cm^2) (Fig. 10). Notably, there was a dramatic decrease in PCE from 11.10%, 11.68%, and 11.45% to 7.87%, 8.59%, and 8.34% for TiO_2, SnO_2, and ZnO-based solar cells, respectively. These decreases were attributed to the reduction in V_{OC} for all devices. Additionally, it was observed that FF decreased slightly, unlike J_{sc}, which remained stable across the entire range of variation. This drop in V_{OC} indicates the introduction of recombination centers by the defects, which leads to the recombination of charge carriers [81].

To dive more the energy levels introduced by interface defects can trap and immobilize charge carriers, causing their

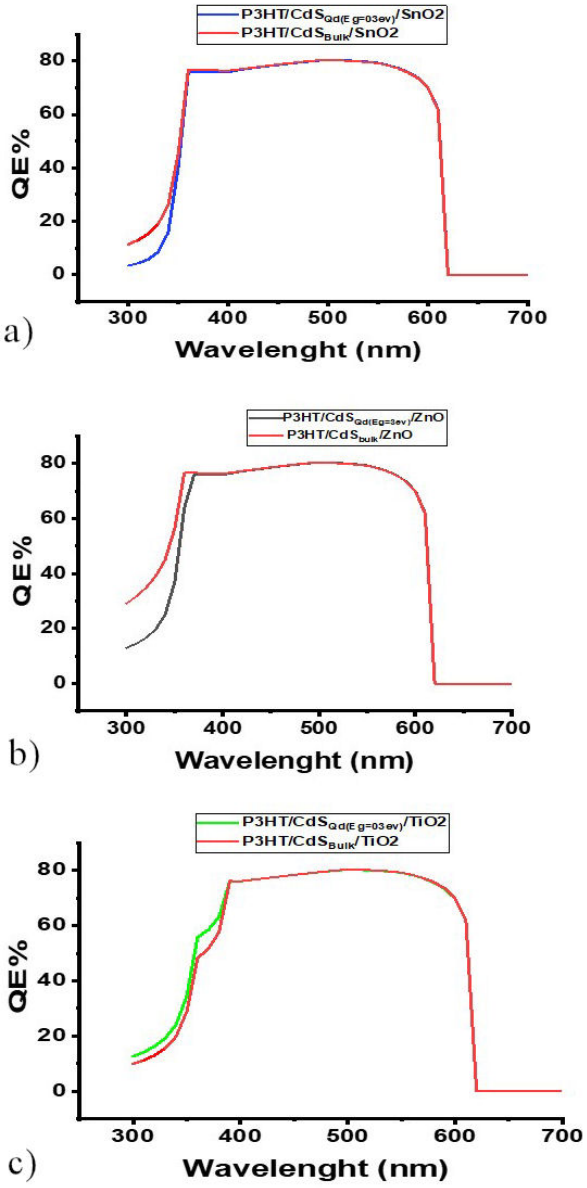

FIGURE 9. CdS Qds Eg variation with Quantum efficiency for ZnO, SnO_2 and TiO_2 based solar cells.

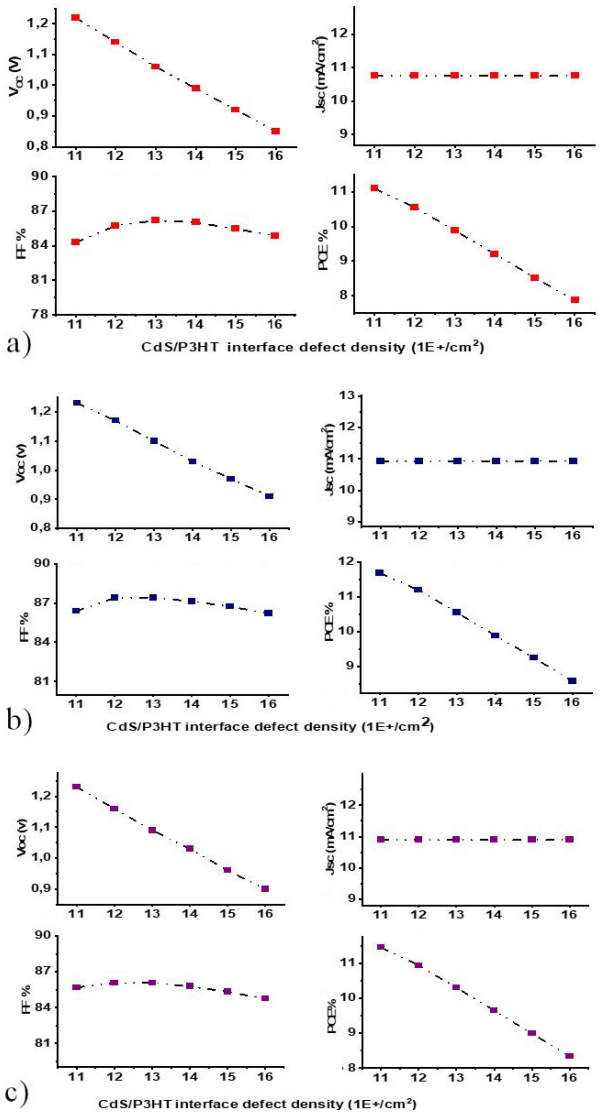

FIGURE 10. P3HT/CdS QDs interface defects variation with respect to V_{OC}, J_{sc}, FF and PCE for a) TiO_2, b) SnO_2 and c) ZnO based solar cells

recombination. The amount of charge carriers available to generate voltage is decreased throughout this recombination process, which eventually has an impact on the device's performance. Increased charge carrier trapping and recombination rates lead to a reduction in the device's efficiency, open-circuit voltage (V_{OC}), and power conversion efficiency (PCE), which are all affected by the density of these defects at the interface [82]. On the other hand, J_{sc} stays constant even in the presence of neutral defects at the interface because it is primarily influenced by the amount of absorbed light and the resulting generation of electron-hole pairs. The quantity of produced charge carriers will not be considerably influenced by the defects at the interface as long as the absorber layer is exposed to the same amount of incident light [83] while FF is more sensitive to the effects of charge transport within the solar cell because it reflects the efficiency of utilizing the generated current for useful work Jmp [84]. Neutral defects at the interface that introduce recombination centers or traps can impede charge transport, leading to a decrease in the actual extracted current and a subsequent reduction in FF [85].

3.6. The effect of electron affinity of P3HT

The impact of varying the electron affinity of P3HT was investigated to explore how adjusting the band alignment could improve solar cell performance. The electron affinity was changed from 3.2 eV to 3.8 eV (Fig. 11), leading to significant alterations in V_{OC}, PCE, J_{sc}, and FF. This variation can be categorized into two ranges: from 3.2 eV to 3.6 eV, where an increase in V_{OC} and FF was observed, subsequently enhancing PCE. During this range, J_{sc} remained relatively stable with only a minor increase. Specifically, V_{OC} improved

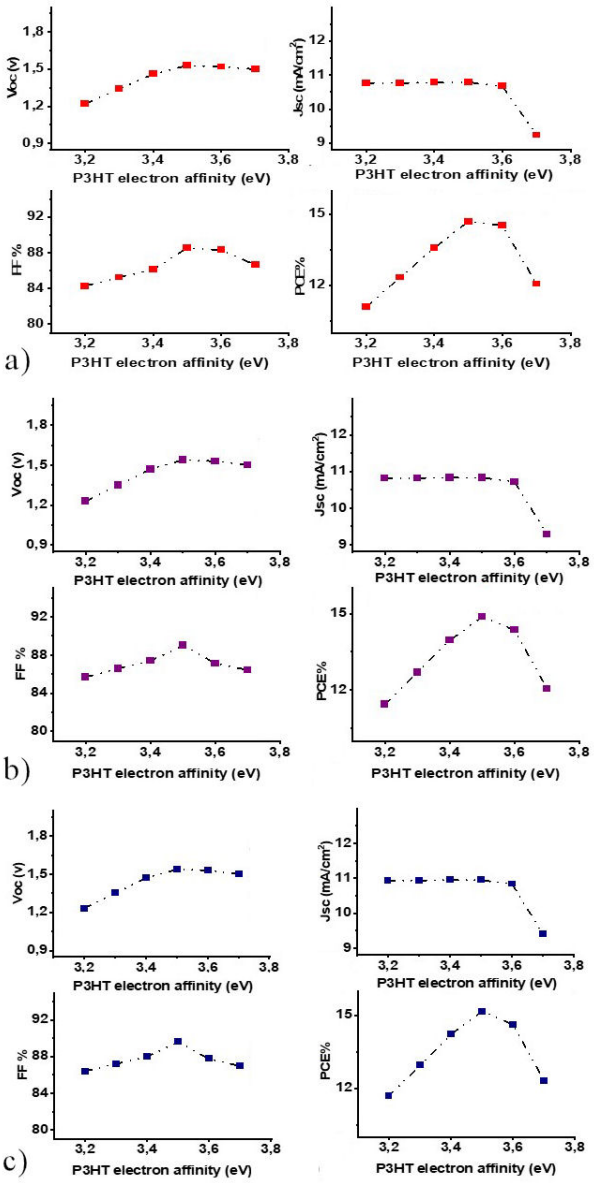

FIGURE 11. P3HT electron affinity variation with respect of V_{OC}, J_{sc}, FF and PCE for a) TiO_2, b) ZnO and c) SnO_2 based solar cells.

from 1.22 V to 1.53 V for TiO_2- based solar cells, and from 1.23 V to 1.54 V for SnO_2 and ZnO-based solar cells. Consequently, PCE increased from 11.10% to 14.7% for TiO_2, from 11.45% to 14.88% for ZnO, and from 11.68% to 15.15% for SnO_2-based solar cells. FF also showed enhancements, rising from 84% to 88%, from 85% to 89%, and from 86.4% to 90% for TiO_2, ZnO, and SnO_2-based solar cells, respectively. Furthermore, J_{sc} exhibited slight changes, increasing from 10.76 mA/cm^2 to 10.79 mA/cm^2, from 10.81 mA/cm^2 to 10.83 mA/cm^2, and from 10.93 mA/cm^2 to 10.95 mA/cm^2.to understand this, Modifying the electron affinity, leading to different values, frequently results in an enhancement of band alignment [86]. This improvement typically signifies that the energy levels of the materials are better suited for aiding the movement of charge carriers and minimizing recombination. Such alignment usually has a positive effect on the overall efficiency of the solar cell [87].

This effect is particularly noticeable between P3HT and the metal contact because, upon the interaction of a metal with a semiconductor, a barrier forms at the boundary between the two materials. This barrier plays a pivotal role in controlling the current flow. In our context, an Ohmic contact exists, and when the electron affinity is raised, the barrier diminishes, simultaneously leading to a decrease in contact resistance Rc. This alteration contributes to a rise in V_{OC} (open-circuit voltage) and FF (fill factor), thus enhancing the power conversion efficiency (PCE) of the solar cell. Nevertheless, when the electron affinity surpasses 3.6 eV, the nature of the contact shifts from being ohmic to becoming rectifying, resulting in an increase in contact resistance. Consequently, this alteration in the contact type has a notable impact on the parameters of the solar cell, influencing its overall performance [88].

3.7. The effect of metal work function variation

To understand more about the effect of ohmic contact and rectifying contact, the simulation study involves altering the work function of metals that are in contact with P3HT semiconductor where the work function is the energy needed for an electron to be removed from a solid surface [89]. The range of metal work functions studied is from 4.5 eV to 5.7 eV. For metals with a work function ϕ_m lower than 5.2 eV (Fig. 12), there were decreases in solar cell performance due to the formation of a rectifying Schottky barrier at the interface between the P3HT layer and the back electrode. A Schottky barrier is an energy barrier that forms at the metal-semiconductor junction, which can rectify the flow of charge carriers (electrons or holes). In this case, it impedes the movement of holes from the P3HT layer towards the back electrode since it allows current flow in only one direction, blocking the flow in the opposite direction [90]. This obstruction leads to an increase in contact resistance, making it more difficult for charge carriers to move through the junction. Additionally, the barrier can lead to occurrences of carrier recombination and this barrier decrease with the increase of work function that is why there was an increasing trend in V_{OC}, J_{sc}, FF and PCE [88]. On the other hand, when the metal work function values are equal to or greater than 5.3 eV, all parameters of the device exhibit a consistent saturation trend since it shifts from forming rectifying contact to ohmic contact which allows for easy movement of charge carriers (in this case, holes) between the layers. An ohmic contact has minimal energy barriers and results in efficient current flow without significant energy loss due to recombination or resistance, Ohmic contacts are preferred for solar cells as they have low contact resistance, allowing for efficient charge carrier extraction thus there was the maximum of solar cell performance results [91].

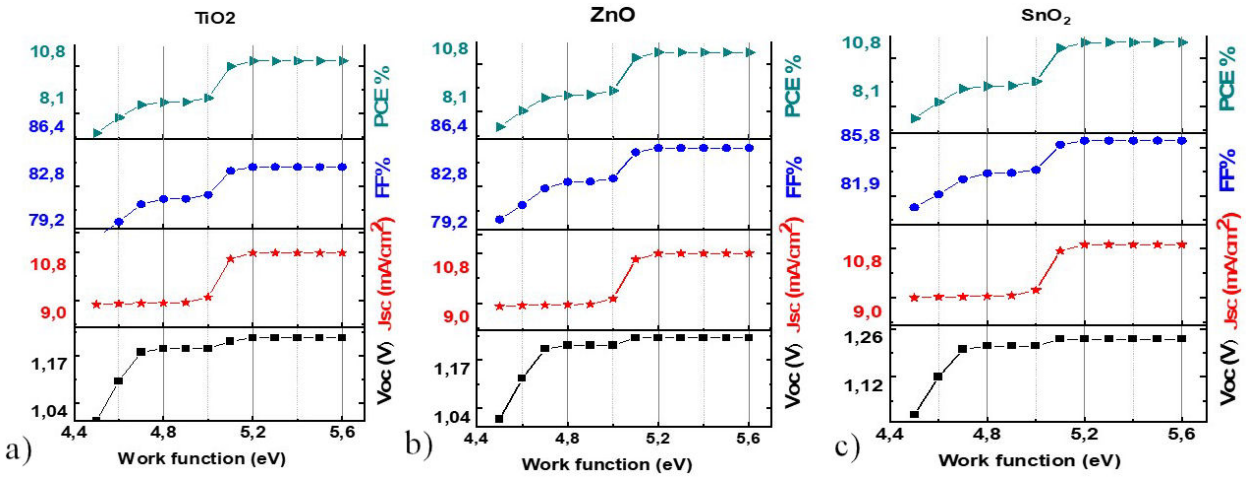

FIGURE 12. Work function variation with respect to V_{OC}, J_{sc}, FF and PCE for TiO_2, ZnO and SnO_2 based solar cells.

4. Conclusion

This study has provided valuable insights into the potential modifications that can occur in the properties of P3HT/CdS Qds when producing solar cells on a commercial scale. To achieve the desired structure of FTO/metal oxide/CdSQds/pt, the SCAPS-1D software package was employed for optimization and design purposes. Enhancements in the cell's performance were achieved through adjustments to various factors, including thickness, interface defect, P3HT bulk defect, P3HT electron affinity, alteration of the CdS Qds gap, and adjustment of the metal work function. The analysis reveals that to enhance performance, it is crucial to align the electron affinity of P3HT with a value of 3.6 eV and reduce the bulk defect density of P3HT to 10^{10} cm^{-3}. Additionally, maintaining an interface defect density of 10^5 cm^{-2} in the P3HT/CdS Qds junction and utilizing a metal work function of 5.65 eV for achieving a good ohmic contact are essential. Furthermore, optimizing the metal oxide thickness to 500 nm and the P3HT layer thickness to 1000 nm, along with setting the CdS Qds gap at 3.00 eV, are necessary steps to potentially achieve a performance level of 18%. Finally using numerical simulations for solar cell designs offers companies crucial insights, ultimately leading to time and cost savings. To complement the theoretical aspects discussed in this research, it is recommended to pursue an experimental approach to evaluate the performance of model QDSC solar cells.

Acknowledgments

This research received support from the Algerian Ministry of Higher Education and Scientific Research.

Author Contributions

All authors contributed to the conception and design of the study. And all authors reviewed and approved the final manuscript.

Funding

This work was financially supported by the Directorate General for Scientific Research and Technological Development of the Algerian Ministry of Higher Education and Scientific Research.

Data availability

No data availability statement is applicable.

Declarations

Conflict of interest

The authors affirm that they do not have any conflicts of interest to disclose.

1. C. Tamin *et al.*, Investigation of absorber and heterojunction in the pure sulphide kesterite, *Boletín de la Sociedad Española de Cerámica y Vidrio* **60** (2021) 380, https://doi.org/10.1016/j.bsecv.2020.05.004.
2. Naureen *et al.*, A Comparative Study of Quantum Dot Solar Cell with Two Different ETLs of WS2 and IGZO Using SCAPS-1D Simulator, *Solar* **2** (2022) 341, https://doi.org/10.3390/solar2030020.
3. N. Kant and P. Singh, Review of next generation photovoltaic solar cell technology and comparative materialistic development, *Materials Today: Proceedings* **56** (2022) 3460, https://doi.org/10.1016/j.matpr.2021.11.116.
4. A. S. Rasal *et al.*, Stability of quantum dot-sensitized solar cells: A review and prospects, *Nano Energy* **94** (2022) 106854, https://doi.org/10.1016/j.nanoen.2021.106854.

5. G. Shilpa *et al.,* Recent advances in the development of high efficiency quantum dot sensitized solar cells (QDSSCs): A review, *Materials Science for Energy Technologies* **6** (2023) 533, https://doi.org/10.1016/j.mset.2023.05.001.

6. N. Chung *et al.*, Quantum Dot Sensitized Solar Cell: Photoanodes, Counter Electrodes, and Electrolytes, *Molecules* **26** (2021) 2638, https://doi.org/10.3390/molecules26092638.

7. D. H. Phuc and H. T. Tung, Quantum dot sensitized solar cell based on the different photoelectrodes for the enhanced performance, *Solar Energy Materials and Solar Cells* **196** (2019) 78, https://doi.org/10.1016/j.solmat.2019.03.038.

8. D. H. Phuc and H. T. Tung, The effect of thickness on the performance of CdSe:Cu2+ -quantum dot-sensitized solar cells, *Applied Physics A* **124** (2018) 731, https://doi.org/10.1007/s00339-018-2150-z.

9. A. K. Ogundele and G. T. Mola, Ternary atoms alloy quantum dot assisted hole transport in thin film polymer solar cells, *Journal of Physics and Chemistry of Solids* **171** (2022) 110999, https://doi.org/10.1016/j.jpcs.2022.110999.

10. R. Katwal, A review: Properties and diverse applications of smart magnetic quantum dots, *Nano-Structures & Nano- Objects* **35** (2023) 101001, https://doi.org/10.1016/j.nanoso.2023.101001.

11. Z. Abdulghani, A. Najm, and A. E. A. Holi, Numerical simulation of quantum dots as a buffer layer in CIGS solar cells: a comparative study, *Scientific Reports* **12** (2022) 8099, https://doi.org/10.1038/s41598-022-12234-0.

12. Z. Abdulghani, A. Najm, A. Holi, A. Al-Zahrani, K. Al-Zahrani, and H. Moria, Numerical simulation of quantum dots as a buffer layer in CIGS solar cells: a comparative study, *Scientific Reports* **12** (2022) 8099, https://doi.org/10.1038/s41598-022-12234-0.

13. R. Singh and B. Pal, Study of excited charge carrier's lifetime for the observed photoluminescence and photocatalytic activity of CdS nanostructures of different shapes, *Journal of Molecular Catalysis A: Chemical* **371** (2013) 77, https://doi.org/10.1016/j.molcata.2013.01.024.

14. X. Wang, Y. Li, Q. Gao, J. Kong, S. Yuan, and S. Wu, (NH4)2S-induced improvement of CdS buffer layer for 15.52% efficiency solution-processed CIGS solar cell, *Journal of Materials Science: Materials in Electronics* **34** (2023) 1680, https://doi.org/10.1007/s10854-023-11097-z.

15. C. Zhou *et al.,* Controllable synthesis of CdS quantum dots and their photovoltaic application on quantum-dot-sensitized ZnO nanorods, *Journal of Solid State Electrochemistry* **20** (2016) 533, https://doi.org/10.1007/s10008-015-3075-5.

16. D. Behar *et al.,* Electrodeposition of CdS quantum dots and their optoelectronic characterization by photoelectrochemical and scanning probe spectroscopies, *Superlattices and Microstructures* **25** (1999) 601, https://doi.org/10.1006/spmi.1999.0696.

17. K. Veerathangam, M. Senthil Pandian, and P. Ramasamy, Influence of SILAR deposition cycles in CdS quantum dot-sensitized solar cells, *Journal of Materials Science: Materials in Electronics* **29** (2018) 7318, https://doi.org/10.1007/s10854-018-8721-0.

18. K. Aruchamy *et al.,* Gel Polymer Electrolytes: Advancing Solid-State Batteries for High-Performance Applications, *Gels* **9** (2023) 585, https://doi.org/10.3390/gels9070585.

19. N. Wang *et al.*, Current Progress in Solid-State Electrolytes for Dye-Sensitized Solar Cells: A Mini-Review, *Journal of Electronic Materials* **49** (2020) 7085, https://doi.org/10.1007/s11664-020-08483-2.

20. B. Korir, J. Kibet, and S. Ngari, Simulated performance of a novel solid-state dye-sensitized solar cell based on phenyl-C61-butyric acid methyl ester (PC61BM) electron transport layer, *Optical and Quantum Electronics* **53** (2021) 368, https://doi.org/10.1007/s11082-021-03013-8.

21. D. Sharma, R. Mehra, and B. Raj, Comparative study of hole transporting layers commonly used in high-efficiency perovskite solar cells, *Journal of Materials Science* **57** (2022) 21172, https://doi.org/10.1007/s10853-022-07958-3.

22. D. Ti *et al.,* Conjugated Polymers as Hole Transporting Materials for Solar Cells, *Chinese Journal of Polymer Science* **38** (2020) 449, https://doi.org/10.1007/s10118-020-2369-y.

23. J. Liu *et al.*, Toward efficient hybrid solar cells comprising quantum dots and organic materials: progress, strategies, and perspectives, *Journal of Materials Chemistry A* **11** (2023) 1013, https://doi.org/10.1039/D2TA07671C.

24. N. Balis *et al.*, A solid-state hybrid solar cell made of nc-TiO2, CdS quantum dots, and P3HT with 2-amino-1- methylbenzimidazole as an interface modifier, *The Journal of Physical Chemistry C* **115** (2011) 10911, https://doi.org/10.1021/jp2022264.

25. J. Qian *et al*., P3HT as hole transport material and assistant light absorber in CdS quantum dots-sensitized solid-state solar cells, *Chemical Communications* **47** (2011) 6461, https://doi.org/10.1039/C1CC11595B.

26. S. Yılmaz *et al.,* Fabrication of CdS nanospheres-based hybrid solar cells having increased efficiency, *Applied Physics A* **128** (2022) 183, https://doi.org/10.1007/s00339-022-05317-2.

27. Y. Li *et al.,* Performance improvement of P3HT/TiO2 coaxial heterojunction polymer solar cells by introducing a CdS interface modifier, *Journal of Solid-State Chemistry* **196** (2012) 349, https://doi.org/10.1016/j.jssc.2012.06.041.

28. Y. Nan *et al.,* Performance enhancement of CdS nanorod arrays/ P3HT hybrid solar cells via N719 dye interface modification, *Chinese Journal of Polymer Science* **31** (2013) 879, https://doi.org/10.1007/s10118-013-1274-z.

29. J. Santos-Cruz *et al.,* Divulging the role of Cu doped CdS nanocrystals as an electron acceptor in hybrid solar cells, *Materials Letters* **312** (2022) 131719, https://doi.org/10.1016/j.matlet.2022.131719.

30. S. Prabakaran *et al.,* Synergistic effect and enhanced electrical properties of TiO2/SnO2/ZnO nanostructures as electron extraction layer for solar cell application, *Applied Surface Science* **498** (2019) 143702, https://doi.org/10.1016/j.apsusc.2019.143702.

31. K. Ellmer, R. Mientus, and S. Seeger, Metallic Oxides (ITO, ZnO, SnO2, TiO2), In D. Levy and E. Castellón, eds., *Transparent Conductive Materials* (Wiley-VCH, 2018), https://doi.org/10.1002/9783527804603.ch2_1.

32. N. Sultana *et al.,* Unveiling the structures and electronic properties of CH3NH3PbI3 interfaces with TiO2, ZnO, and SnO2: a first-principles study, *Journal of Materials Science* **54** (2019) 13594, https://doi.org/10.1007/s10853-019-03867-0.

33. M. I. Ahamed, M. Ahamed, and R. Muthaiyan, Modelling of density of states and energy level of chalcogenide quantum dots, *International Review of Applied Sciences and Engineering* **13** (2021) 42, https://doi.org/10.1556/1848.2021.00288.

34. V. G. Litovchenko and A. A. Grygoriev, Determination of the electron affinity (work function) of semiconductor nanocrystals, *Ukrains'kyi Fizychnyi Zhurnal* **52** (2007) 897

35. E. Kuçur *et al.,* Determination of Defect States in Semiconductor Nanocrystals by Cyclic Voltammetry, *The Journal of Physical Chemistry B* **109** (2005) 20355, https://doi.org/10.1021/jp053891b.

36. L. E. Greene *et al.,* ZnOTiO2 CoreShell Nanorod/P3HT Solar Cells, *The Journal of Physical Chemistry C* **111** (2007) 18451, https://doi.org/10.1021/jp077593l.

37. F. Wu *et al.,* Changes of Voc in hybrid solar cells by TiO2 nanoarray with different crystallinity of shell, *Journal of The Electrochemical Society* **161** (2014) H593, https://doi.org/10.1149/2.0161410jes.

38. S. S. Williams *et al.,* Nanostructured TitaniaPolymer Photovoltaic Devices Made Using PFPE-Based Nano molding Techniques, *Chemistry of Materials* **20** (2008) 5229, https://doi.org/10.1021/cm800729q.

39. M. K. Hossain *et al.,* Numerical analysis in dft and scaps- 1d on the influence of different charge transport layers of cspbbr3 perovskite solar cells, *Energy & Fuels* **37** (2023) 6078, https://doi.org/10.1021/acs.energyfuels.3c00035.

40. M. B. Rahman *et al.,* Selection of a compatible electron transport layer and hole transport layer for the mixed perovskite FA0.85Cs0.15Pb (I0.85Br0.15)3, towards achieving novel structure and high-efficiency perovskite solar cells: a detailed numerical study by SCAPS-1D, *RSC Advances* **13** (2023) 17130, https://doi.org/10.1039/D3RA02170J.

41. S. Barthwal *et al.,* Band offset engineering in antimony sulfide (Sb2S3) solar cells, using SCAPS simulation: A route toward PCE $>$ 10%, *Optik* **282** (2023) 170868, https://doi.org/10.1016/j.ijleo.2023.170868.

42. Z. Li, P. Graziosi, and N. Neophytou, Electron and Hole Mobility of SnO2 from Full-Band Electron-Phonon and Ionized Impurity Scattering Computations, *Crystals* **12** (2022) 1591, https://doi.org/10.3390/cryst12111591.

43. W. Henni *et al.,* Effect of introducing Al2O3 as a tunnelling layer into p-CBTS/n-CdS heterojunction solar cells, *Journal of Computational Electronics* **22** (2023) 897, https://doi.org/10.1007/s10825-023-02031-x.

44. N. Jayah *et al.,* High electron mobility and low carrier concentration of hydrothermally grown ZnO thin films on seeded a-plane sapphire at low temperature, *Nanoscale Research Letters* **10** (2015) 7, https://doi.org/10.1186/s11671-014-0715-0.

45. B. Walker *et al.,* Solution-processed CdS transistors with high electron mobility, *RSC Advances* **4** (2014) 3153, https://doi.org/10.1039/C3RA44436H.

46. V. Skrypnychuk *et al.,* Ultrahigh Mobility in an Organic Semiconductor by Vertical Chain Alignment, *Advanced Materials* **28** (2016) 2359, https://doi.org/10.1002/adma.201503422.

47. K. Mamta, Maurya, and V. Singh, Sb2Se3 as an HTL for Mo/Sb2Se3/Cs2TiF6/TiO2 solar structure: performance evaluation with SCAPS-1D, *Heliyon* **8** (2022) e10925, https://doi.org/10.1016/j.heliyon.2022.e10925.

48. S. Zyoud *et al.,* Numerical Modeling of High Conversion Efficiency FTO/ZnO/CdS/CZTS/MO Thin Film-Based Solar Cells: Using SCAPS-1D Software, *Crystals* **11** (2021) 1468, https://doi.org/10.3390/cryst11121468.

49. L. Chen, C. Fang, and W. Liu, Influence of Absorption Layer Thickness on the Performance of CIGS Solar Cells, *IOP Conference Series: Earth and Environmental Science* **440** (2020) 032051, https://doi.org/10.1088/1755-1315/440/3/032051.

50. R. Street, K. Song, and S. Cowan, Influence of series resistance on the photocurrent analysis of organic solar cells, *Organic Electronics* **12** (2011) 244, https://doi.org/10.1016/j.orgel.2010.11.012.

51. J. R. Tumbleston *et al.,* Nonideal parasitic resistance effects in bulk heterojunction organic solar cells, *Journal of Applied Physics* **108** (2010) 084514, https://doi.org/10.1063/1.3494100.

52. R. Jeyakumar *et al.,* Influence of Electron Transport Layer (TiO2) Thickness and Its Doping Density on the Performance of CH3NH3PbI3-Based Planar Perovskite Solar Cells, *Journal of Electronic Materials* **49** (2020) 3533, https://doi.org/10.1007/s11664-020-08041-w.

53. M. Hossain *et al.,* An extensive study on multiple ETL and HTL layers to design and simulation of high-performance leadfree CsSnCl3-based perovskite solar cells, *Scientific Reports* **13** (2023) 2521, https://doi.org/10.1038/s41598-023-28506-2.

54. H. Chen *et al.,* Towards high-efficiency planar heterojunction antimony sulfide solar cells, *Optical Materials* **121** (2021) 111556, https://doi.org/10.1016/j.optmat.2021.111556.

55. B. Korir, J. Kibet, and S. Ngari, Computational Simulation of a Highly Efficient Hole Transport-Free Dye-Sensitized Solar Cell Based on Titanium Oxide (TiO2) and Zinc Oxysulfide (ZnOS) Electron Transport Layers, *Journal of Electronic Materials* **50** (2021) 7259, https://doi.org/10.1007/s11664-021-09250-7.

56. T. Ouslimane *et al.,* Impact of absorber layer thickness, defect density, and operating temperature on the performance of MAPbI3 solar cells based on ZnO electron transporting material, *Heliyon* **7** (2021) e06379, https://doi.org/10.1016/j.heliyon.2021.e06379.

57. H.-J. Du, W.-C. Wang, and J.-Z. Zhu, Device simulation of lead-free CH3NH3SnI3 perovskite solar cells with high efficiency, *Chinese Physics B* **25** (2016) 108802, https://doi.org/10.1088/1674-1056/25/10/108802.

58. D. KC *et al.,* Impact of Different Antireflection Layers on Cadmium Telluride (CdTe) Solar Cells: a PC1D Simulation Study, *Journal of Electronic Materials* **50** (2021) 2199, https://doi.org/10.1007/s11664-020-08696-5.

59. P. Roy *et al.,* Influence of defect density and layer thickness of absorption layer on the performance of tin-based perovskite solar cell, In IOP Conference Series: *Materials Science and Engineering*, **798** (2020) 012020, https://doi.org/10.1088/1757-899X/798/1/012020.

60. E. Danladi *et al.,* Optimization of absorber and ETM layer thickness for enhanced tin-based perovskite solar cell performance using SCAPS-1D software, *Physics Access* **2** (2022) 1, https://doi.org/10.47514/phyaccess.2022.2.1.001.

61. H. Chen *et al.,* Towards high-efficiency planar heterojunction antimony sulfide solar cells, *Optical Materials* **121** (2021) 111556, https://doi.org/10.1016/j.optmat.2021.111556.

62. P. Singh and N. Ravindra, Temperature dependence of solar cell performance-an analysis, *Solar Energy Materials and Solar Cells* **101** (2012) 36, https://doi.org/10.1016/j.solmat.2012.02.019.

63. N. Wu *et al.,* Identifying the cause of voltage and fill factor losses in perovskite solar cells by using luminescence measurements, *Energy Technology* **5** (2017) 1827, https://doi.org/10.1002/ente.201700374.

64. M. Ulum, E. Sesa, and W. Belcher, The effect of active layer thickness on P3HT: PCBM nanoparticulate organic photovoltaic device performance, *In Journal of Physics: Conference Series* **1242** (2019) 012025, https://doi.org/10.1088/1742-6596/1242/1/012025.

65. M. Zidan, T. Ismail, and I. Fahim, Effect of thickness and temperature on flexible organic P3HT: PCBM solar cell performance, *Materials Research Express* **8** (2021) 095508, https://doi.org/10.1088/2053-1591/ac2773.

66. P. Morvillo *et al.,* Effect of the Active Layer Thickness on the Device Performance of Polymer Solar Cells Having [60]PCBM and [70]PCBM as Electron Acceptor, *Energy Procedia* **31** (2012) 69, https://doi.org/10.1016/j.egypro.2012.11.166.

67. A. Umar *et al.,* High Power-Conversion Efficiency of Lead-Free Perovskite Solar Cells: A Theoretical Investigation, *Micromachines* **13** (2022) 2201, https://doi.org/10.3390/mi13122201.

68. R. N. Mohottige and S. P. Kalawila Vithanage, Numerical simulation of a new device architecture for CIGS-based thinfilm solar cells using 1D-SCAPS simulator, *Journal of Photochemistry and Photobiology A: Chemistry* **407** (2021) 113079, https://doi.org/10.1016/j.jphotochem.2020.113079.

69. N. Amin *et al.,* Prospects of back surface field effect in ultra-thin high-efficiency CdS/CdTe solar cells from numerical modeling, *International Journal of Photoenergy 2010* (2011) 578580, https://doi.org/10.1155/2010/578580.

70. F. Jhuma, M. Shaily, and M. Rashid, Towards high-efficiency CZTS solar cell through buffer layer optimization, *Materials for Renewable and Sustainable Energy* **8** (2019) 6, https://doi.org/10.1007/s40243-019-0144-1.

71. F. Rabouw and C. de Mello Donega, Excited-State Dynamics in Colloidal Semiconductor Nanocrystals, *Topics in Current Chemistry* **374** (2016) 58, https://doi.org/10.1007/s41061-016-0060-0.

72. V. Klimov *et al.,* Single-exciton optical gain in semiconductor nanocrystals, *Nature* **447** (2007) 441, https://doi.org/10.1038/nature05839.

73. P. Kumar *et al.,* Synthesis Of Mercaptopropionic Acid Stabilized CdS Quantum Dots for Bioimaging In Breast Cancer, *Advanced Materials Letters* **3** (2012) 471, https://doi.org/10.5185/amlett.2012.icnano.296.

74. H. Abdalmageed, M. Fedawy, and M. Aly, Effect of absorber layer bandgap of CIGS-based solar cell with (CdS/ZnS) buffer layer, *In Journal of Physics: Conference Series*, vol. **2128** (2021) p. 012009, https://doi.org/10.1088/1742-6596/2128/1/012009.

75. A. Chaves *et al.,* Bandgap engineering of two-dimensional semiconductor materials, *npj 2D Materials and Applications* **4** (2020) 29, https://doi.org/10.1038/s41699-020-00162-4.

76. G. A. Nowsherwan *et al.,* Numerical optimization and performance evaluation of ZnPC:PC70BM based dye-sensitized solar cell, *Scientific Reports* **13** (2023) 10431, https://doi.org/10.1038/s41598-023-37486-2.

77. W. Yoon *et al.,* Enhanced Open-Circuit Voltage of PbS Nanocrystal Quantum Dot Solar Cells, *Scientific Reports* **3** (2013) 10413, https://doi.org/10.1038/srep02225.

78. A. Ahmed *et al.,* Performance optimization of CH3NH3Pb(I1-xBrx)3 based perovskite solar cells by comparing different ETL materials through conduction band offset engineering, *Optical Materials* **105** (2020) 109897, https://doi.org/10.1016/j.optmat.2020.109897.

79. T. Hossain *et al.,* Tuning the bandgap of Cd1-xZnxS (x = 0 1) buffer layer and CIGS absorber layer for obtaining high efficiency, *Superlattices and Microstructures* **161** (2022) 107100, https://doi.org/10.1016/j.spmi.2021.107100.

80. Y. Qi *et al.,* Engineering of interface band bending and defects elimination via a Ag-graded active layer for efficient (Cu, Ag)2ZnSn(S, Se)4 solar cells, *Energy Environmental Science* **10** (2017) 2401, https://doi.org/10.1039/C7EE01405H.

81. T. A. Ngoupo, S. Ouédraogo, and J. Ndjaka, Numerical analysis of interface properties effects in CdTe/CdS:O thin film solar cell by SCAPS-1D, *Indian Journal of Physics* **93** (2019) 869, https://doi.org/10.1007/s12648-018-01360-z.

82. S. Z. Haider *et al.,* A comparative study of interface engineering with different hole transport materials for high-performance perovskite solar cells, *Journal of Physics and Chemistry of Solids* **136** (2020) 109147, https://doi.org/10.1016/j.jpcs.2019.109147.

83. F. Izadi *et al.,* Effect of interface defects on high efficient perovskite solar cells, *Optik* **227** (2021) 166061, https://doi.org/10.1016/j.ijleo.2020.166061.

84. D. Gupta, S. Mukhopadhyay, and K. Narayan, Fill factor in organic solar cells, *Solar Energy Materials and Solar Cells* **94** (2010) 1309, https://doi.org/10.1016/j.solmat.2008.06.001.

85. T. Song, A. Kanevce, and J. R. Sites, Emitter/absorber interface of CdTe solar cells, *Journal of Applied Physics* **119** (2016) 233104, https://doi.org/10.1063/1.4953820.

86. S. S. Surah *et al.,* Tuning the electronic band alignment properties of TiO2 nanotubes by boron doping, *Results in Physics* **12** (2019) 1725, https://doi.org/10.1016/j.rinp.2019.01.081.

87. T. Ghorbani *et al.,* Influence of affinity, band gap and ambient temperature on the efficiency of CIGS solar cells, *Optik* **223** (2020) 165541, https://doi.org/10.1016/j.ijleo.2020.165541.

88. P. Patel, Device simulation of highly efficient eco-friendly $CH_3NH_3SnI_3$ perovskite solar cell, *Scientific Reports* **11** (2021) 3082, https://doi.org/10.1038/s41598-021-82817-w.

89. L. Lin *et al.,* Work function: Fundamentals, measurement, calculation, engineering, and applications, *Physical Review Applied* **19** (2023) 037001, https://doi.org/10.1103/PhysRevApplied.19.037001.

90. K. Kumari, T. Chakrabarti, and S. K. Sarkar, Metal oxide nanoparticles as an electron-transport layer in perovskite solar cell, *Optical Materials* **142** (2023) 114047, https://doi.org/10.1016/j.optmat.2023.114047.

91. N. Noorasid *et al.,* Improved performance of lead-free Perovskite solar cell incorporated with TiO2 ETL and CuI HTL using SCAPs, *Applied Physics A* **129** (2023) 132, https://doi.org/10.1007/s00339-022-06356-5.